Giant negative linear compressibility in zinc dicyanoaurate

Andrew B. Cairns [*], Jadna Catafesta [† ‡], Claire Levelut [‡], Jérôme Rouquette [†], Arie can der Lee [§], Lars Peters [¶], Amber L. Thompson [*], Vladimir Dmitriev [‖], Julian Haines [†], and Andrew L. Goodwin [**]

[*]Department of Chemistry, University of Oxford, Inorganic Chemistry Laboratory, South Parks Road, Oxford, OX1 3QR, United Kingdom,[†]Institut Charles Gerhardt, Équipe C2M, UMR–CNRS 5253, Université Montpellier 2, Place E. Bataillon, 34095, Montpellier Cedex 5, France,[‡]Laboratoire Charles Coulomb, UMR–CNRS 5221, Université Montpellier 2, Place E. Bataillon, 34095 Montpellier Cedex 5, France,[§]Institut Européen des Membranes de Montpellier, UMR–CNRS 5635, Université Montpellier 2, 300 Avenue Prof. E. Jeanbrau, 34095 Montpellier, Cedex 5, France,[¶]Institut für Kristallographie, RWTH Aachen, Jaegerstrasse 17-19, 52066 Aachen, Germany, and [‖]ESRF, Polygone Scientifique Louis Néel, 6 rue Jules Horowitz, 38000 Grenoble, France

Submitted to Nature Materials

The counterintuitive phenomenon of negative linear compressibility (NLC) is a highly-desirable but rare property exploitable in the development of artificial muscles (*1*), actuators (*2*) and next-generation pressure sensors (*3*). In all cases, material performance is directly related to the magnitude of intrinsic NLC response. Here we show the molecular framework material zinc(II) dicyanoaurate(I), $Zn[Au(CN)_2]_2$, exhibits the most extreme and persistent NLC behaviour yet reported: under increasing hydrostatic pressure its crystal structure expands in one direction at a rate that is an order of magnitude greater than both the typical contraction observed for common engineering materials (*4*) and also the anomalous expansion in established NLC candidates (*3*). This extreme behaviour arises from the honeycomb-like structure of $Zn[Au(CN)_2]_2$ coupling volume reduction to uniaxial expansion (*5*), and helical Au...Au "aurophilic" interactions (*6*) accommodating abnormally-large linear strains by functioning as supramolecular springs.

For nearly all known materials, an increase in hydrostatic pressure results in a shortening of their linear dimensions. The magnitude of this response can be compared *via* the isothermal compressibilities $K_\ell = -(\partial \ln \ell/\partial p)_T$, defined in terms of the relative rate of change of length ℓ with respect to pressure. Typical linear compressibilities for engineering materials such as metals, alloys and ceramics are $K_\ell \sim 5\,\mathrm{TPa}^{-1}$ (*7*) (*i.e.*, 0.5% reduction in length for each 1 GPa increase in pressure). In contrast, for the handful of materials known to exhibit NLC, one or more of the compressibilities actually takes a negative value. For many years, only 13 NLC compounds had been identified (*3*) and the strongest effect observed amongst these long-established, canonical NLC systems was $K_{\mathrm{NLC}} = -1.2\,\mathrm{TPa}^{-1}$ for trigonal Se (*8*). So in general NLC is much weaker than the typical positive compressibilities of ordinary materials. In seeking to develop systems with the strongest possible NLC coefficients, an emerging approach is to exploit specific geometric motifs that inherently favour NLC. This strategy takes inspiration from the close relationship between geometry and anomalous mechanical response observed widely in artificial and biological systems alike—from the inverse honeycombs responsible for negative Poisson ratios in so-called "auxetic" foams (*9–11*) to the helical tendon arrays responsible for locomotion in caecilian tetrapods (*12*). Using this approach, two recent reports of stronger NLC effects exploit structures with "wine-rack" topologies: methanol monohydrate ($K_{\mathrm{NLC}} = -2.6(3)\,\mathrm{TPa}^{-1}$) (*13*) and ammonium zinc formate ($K_{\mathrm{NLC}} = -1.8(8)\,\mathrm{TPa}^{-1}$) (*14*). In these systems, volume reduction is accommodated by simultaneous compression and expansion of the crystal lattice in orthogonal directions (*i.e.* "folding-up" of the wine-rack (*3*)). Even more extreme responses are accessible by exploiting the dependency of magnitude of mechanical response on the ease with which geometric flexing can take place (*15*). The use of extended molecular linkers that are capable of accommodating large geometry changes has recently led to record NLC effects in wine-rack-like molecular frameworks $[Fe(dpp)_2(NCS)_2]\cdot$py (dpp = dipyrido[3,2-a:2′3′-c]phenazine, py = pyridine) and $KMn[Ag(CN)_2]_3$, for which $K_{\mathrm{NLC}} = -10.3(20)\,\mathrm{TPa}^{-1}$ and $-12.0(8)\,\mathrm{TPa}^{-1}$, respectively, over the pressure range 0–2.2 GPa (*16, 17*).

In the absence of a structural phase transition, it is a thermodynamic requirement that *intrinsic* volume compressibility be positive (*18, 19*) (the possible exception here arises in meta-materials where judiciously-chosen pairwise potentials can result in an effective negative volume compressibility (*20*)); consequently the exis-

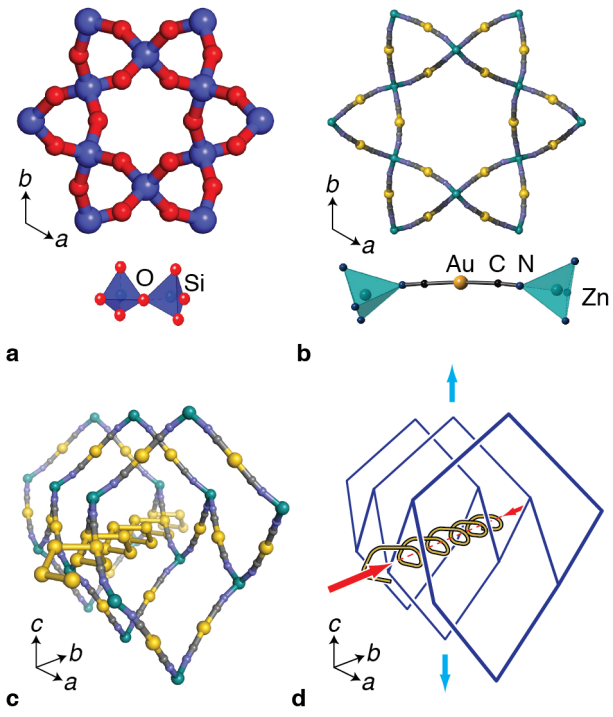

Fig. 1. The β-quartz-like framework structure of $Zn[Au(CN)_2]_2$ functions as a "molecular honeycomb" to give giant negative linear compressibility. a A representation of the crystal structure of β-quartz viewed down its hexagonal axis; the network is assembled from SiO_4 tetrahedra connected at their vertices. **b** One of the six β-quartz-like nets of $Zn[Au(CN)_2]_2$ viewed down its crystallographic c-axis; this framework consists of ZnN_4 tetrahedra connected via flexible dicyanoaurate (N–C–Au–C–N) molecular linkers. **c** A representation of the net shown in **b** from an alternate view that highlights the honeycomb-like nature of its hexagonal pores and also the cross-bracing effect of helical aurophilic chains running perpendicular to the **c** crystal axis. **d** The mechanism of NLC in $Zn[Au(CN)_2]_2$ involves rapid compression of the aurophilic helices, which is transferred to an expansion of the framework in the **c** direction *via* flexing of the honeycomb-like channels.

[**]andrew.goodwin@chem.ox.ac.uk

tence of NLC implies stronger positive linear compressibility (PLC) in directions perpendicular to the NLC axis. Indeed it can be shown for simple uniaxial systems that the full mechanical response is determined by (i) framework geometry and (ii) the magnitude of this positive compressibility (see Supplementary Information). So an important consideration for maximising NLC is ensuring that any interactions in these PLC directions are as compressible as possible. In $KMn[Ag(CN)_2]_3$, for example, the relevant motif is a kagome net of Ag...Ag "argentophilic" interactions. These interactions are already one of the most deformable known, being similar in mechanical strength to the dispersive "bonds" of solid Xe (*21*). So the challenge to the materials chemist becomes how one might engineer a material that is even more compressible than these weakest of interactions, and then translate that large compressibility into extreme NLC behaviour.

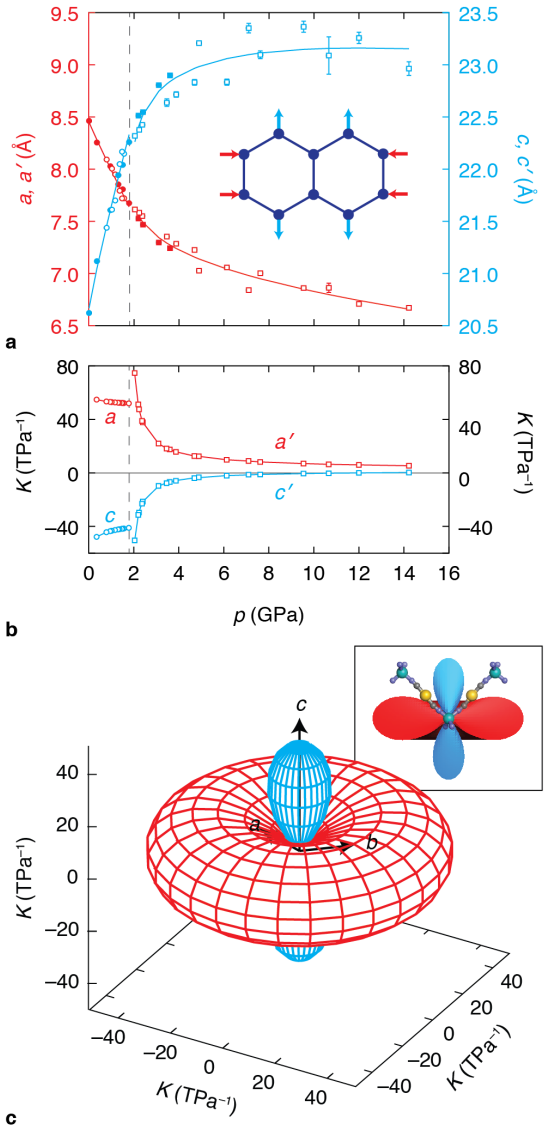

Fig. 2. The compressibility of $Zn[Au(CN)_2]_2$ is quantified by the variation in crystallographic unit-cell parameters. a Lattice parameter changes observed during hydrostatic compression of zinc dicyanoaurate: a (red), c (blue), single-crystal x-ray diffraction (filled markers), powder x-ray diffraction (open markers), ambient phase (circles) and high-pressure phase (squares). The approximate location of the phase I/II transition is indicated by a dashed vertical line. Reduced lattice parameters $a' = a/2, c' = c/2$ have been used for phase-II data in order to enable direct comparison with phase-I lattice parameters. The inset shows a schematic representation of the compression mechanism for hexagonal honeycomb: compression in one direction (red) is coupled to an expansion in a perpendicular direction (blue). **b** Corresponding lattice compressibilities calculated from the data in **a** for the same pressure range. **c** The compressibility indicatrix of the ambient phase of $Zn[Au(CN)_2]_2$-I, showing the spatial orientation of strong positive and negative linear compressibility axes (colours as above) (*26*). The Zn–N–C–Au–C–N–Zn linkages are oriented only along directions for which the uniaxial compressibility vanishes (see inset to **c**, which shows a cross-section of the indicatrix on which two representative linkage orientations are superimposed).

Here we investigate the piezo-mechanical response of $Zn[Au(CN)_2]_2$, a framework material in which tetrahedral Zn^{2+} centres are connected by almost-linear dicyanoaurate $(NC–Au–CN)^-$ linkages (*22–24*). Four polymorphs of this material are known (*23*); our study focuses on the α-polymorph, which is the form most readily synthesised as either a phase-pure powder or as large single-crystals. The topology of this particular $Zn[Au(CN)_2]_2$ framework is identical to that of β-quartz, with the increased Zn...Zn separation allowing sixfold interpenetration (Fig. 1a, b). Cross-bracing these six interpenetrating honeycomb-like nets are sets of weakly-attractive aurophilic interactions ($30 < \Delta H_{Au\ldots Au} \sim \Delta H_{Ag\ldots Ag} < 50\,\mathrm{kJ\,mol^{-1}}$ (*25*)) that form helical chains oriented perpendicular to the **c** crystal axis and which are responsible for a strong luminescent response (*23, 24*) (Fig. 1c). The hexagonal crystal symmetry means that the compressibility of $Zn[Au(CN)_2]_2$ is completely described by the pressure-dependence of the a and c lattice parameters. Using a combination of single-crystal and powder X-ray diffraction we observe strong positive compressibility within the (001) crystal plane ($K_a = +52(6)\,\mathrm{TPa^{-1}}$) together with a remarkably strong NLC effect parallel to the **c** crystal axis ($K_c = -42(5)\,\mathrm{TPa^{-1}}$) (Fig. 2) (*26*). Both effects persist throughout the stability field of the ambient phase ($0 < p < 1.8\,\mathrm{GPa}$); full details of our structural refinements are given in the Supplementary Information. We are proposing the use of the term "giant" to demarcate NLC behaviour—such as we observe here—that is an order of magnitude stronger than that of the canonical systems described above (*i.e.*, $K_\ell < -30\,\mathrm{TPa^{-1}}$) (*3*) and which persists for the *ca* 1 GPa pressure range associated with typical high-pressure applications (*27*).

Because the Zn centres occupy special positions within the unit cell (*22*), and because these positions correspond to the nodes of the quartz-like networks, then the geometric response of the framework to increasing pressure is unambiguously determined by the lattice parameter variation (see Supplementary Information). In particular, the volume reduction required thermodynamically is accommodated by narrowing of the honeycomb-like channels parallel to the $\langle 100 \rangle$ axes (hence PLC in these directions). This narrowing of channels results in elongation of the crystal along the perpendicular [001] axis by virtue of a well-understood mechanical property of honeycombs (of which the β-quartz net is a three-dimensional analogue)—namely, their large and negative elastic compliance S_{13} that translates horizontal compression into vertical expansion (*5*). This effect is conceptually similar to the wine-rack mechanism discussed above; in both cases the assumption is made that compression involves network hingeing in preference to deformation of the framework struts (see Supplementary Information for further discussion). We can be sure that the mechanical behaviour we observe here is indeed a geometric effect and does not involve significant changes to bonding interactions in the solid because the set of directions for which K_ℓ vanishes actually includes the Zn–NC–Au–CN–Zn vectors (Fig. 2c). Hence the edge lengths of the covalent network are essentially unaffected by pressure; it is only the network angles that vary. In this sense the geometric response of $Zn[Au(CN)_2]_2$ is very similar to that of $KMn[Ag(CN)_2]_3$ and the other "wine-rack" NLC materials. So the question remains: why is NLC so extreme in this particular case?

We proceed to demonstrate that it is the helical nature of the Au...Au interactions that is crucial in driving giant NLC in

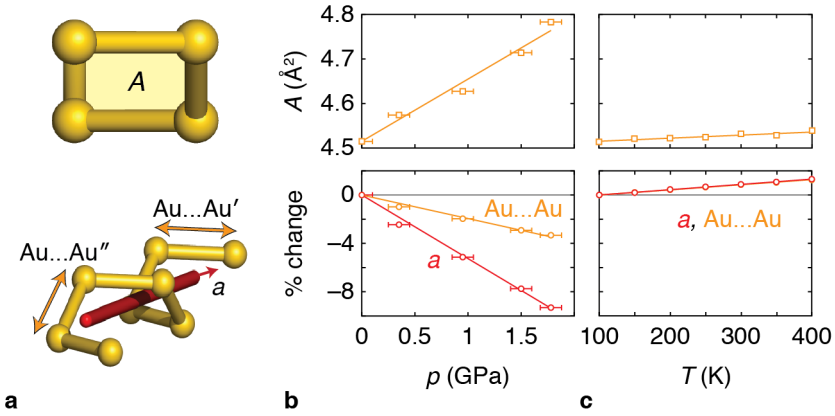

Fig. 3. Compressibility enhancement in $Zn[Au(CN)_2]_2$ *via* "spring"-like deformations. a By analogy with macroscopic spring mechanics, the crucial structural parameters that describe the mechanical state of the aurophilic helices found in $Zn[Au(CN)_2]_2$ are its pitch (length per turn, given by the lattice parameter a) and its cross-sectional area A. The value of A depends on the magnitude and orientation of the two crystallographically-independent Au. . .Au vectors, and is independent of the lattice parameters. **b** Under hydrostatic compression, the a lattice parameter decreases approximately three times more rapidly than does the average Au. . .Au distance; this discrepancy is accommodated by an increase in the cross-sectional area A. The helix acts like a spring under compression, allowing a magnitude of compressibility that would not otherwise be attainable. **c** The thermal expansion behaviour of $Zn[Au(CN)_2]_2$ is much more moderate because the entire "spring" simply expands on heating at the rate expected for aurophilic interactions. The thermal variation in both the lattice parameter a and the average Au. . .Au separation are shown in the bottom panel, but are almost indistinguishable because of their close similarity.

$Zn[Au(CN)_2]_2$. Just as a steel spring is profoundly more compressible than steel itself, so too might one expect Au. . .Au helices to be more compressible than the individual interactions. And because it is the repeat length of the helix—rather than the average Au. . .Au separation—that determines the lattice parameters, the $Zn[Au(CN)_2]_2$ crystal lattice can be more compressible than any of its constituent chemical bonds. This argument is strongly supported by the results of our variable-pressure crystallographic refinements: (i) the a lattice parameter contracts three times more quickly with increasing pressure than does the average Au. . .Au distance, and (ii) the helix cross-sectional area (which defines an effective helix radius) increases with increasing pressure as expected for a spring mechanism in compression (Fig. 3). So the extreme PLC effect observed along the $\langle 100 \rangle$ directions does not require an equally large change in Au. . .Au distances because any difference is accommodated by a variation in helix radius (Fig. 3a). This situation contrasts that in $KMn[Ag(CN)_2]_3$ where the crystal symmetry demands that the macroscopic PLC behaviour match exactly the average Ag. . .Ag compressibility (*17*). We also find that a spring-like response in $Zn[Au(CN)_2]_2$ is specifically a pressure-induced mechanism, and is not thermally activated: increasing temperature at constant (ambient) pressure simply causes the Au. . .Au distances, the a lattice parameter, and the cross-sectional area A all to increase at the same relatively modest rate expected for aurophilic interactions (Fig. 3d) (*24, 28*).

Thermodynamically, the giant NLC we observe is not sustainable indefinitely. At a critical pressure $p_c \simeq 1.8$ GPa we observe a displacive transition to a $2 \times 2 \times 2$ supercell of enantiomorphic space group symmetry (Fig. 4; see Supplementary Information). The dominant structural change associated with the transition is a set of small concerted rotations of the Zn-centred coordination tetrahedra associated with mode softening at the Brillouin zone boundary (L-point); in particular there is no change to the network connectivity or crystal symmetry, nor are the lattice strains involved particularly large. Interestingly, the effect of this transition on the compressibility behaviour of the ambient phase $Zn[Au(CN)_2]_2$-I can be seen in the pressure derivative B' of its bulk modulus: a third-order Birch-Murnaghan (B-M) fit (*26*) to our $V(p)$ data gives $B' = -1.7(11)$, which indicates—counterintuitively—that the phase becomes mechanically softer on compression (*27, 29*). This softening of vibrational mode frequencies is evident in pressure-dependent spectroscopic measurements, which also reflect the expected symmetry lowering (mode splitting) at the transition pressure (see Supplementary Information). The pressure dependencies of the phonon frequencies revert to positive values in the high-pressure phase, and a second-order B-M fit ($B' \equiv 4$) describes well the phase-II $V(p)$ data. Finally, we note that the close structural relationship between ambient and high-pressure forms means that the NLC effect we observe at low pressures persists in $Zn[Au(CN)_2]$-II despite the structural transition—albeit at a significantly reduced level ($K_c = -6(3)\,\mathrm{TPa}^{-1}$ for the pressure range $1.8 < p < 14.2$ GPa). One generally anticipates a reduction in magnitude of compressibilities at increased pressure, but an additional contributing factor here is the sideways buckling of Au. . .Au helices that likely reduces their effectiveness in accommodating large com-

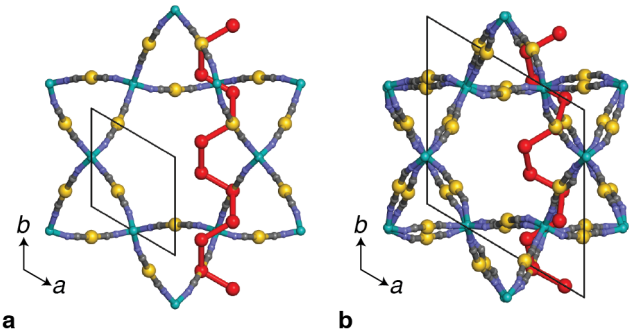

Fig. 4. Relationship between the ambient (I) and high-pressure (II) phases of $Zn[Au(CN)_2]_2$. a The same representation of the β-quartz-like crystal structure of ambient $Zn[Au(CN)_2]_2$ used in Fig. 1b, with the corresponding hexagonal unit cell and one of the aurophilic helices indicated (the latter in red). **b** The high-pressure form $Zn[Au(CN)_2]_2$-II has a unit cell that is doubled along each axis. While the fundamental network connectivity is preserved in the two forms, the high-pressure phase is distinguished by the presence of small concerted tilts of $[ZnN_4]$ tetrahedra that correspond to a soft phonon mode of the parent structure. Aurophilic helices are present in both forms, but are increasingly severely distorted at high pressures (see Supporting Figure 5).

pressibilities.

Perhaps the most immediate application of NLC in $Zn[Au(CN)_2]_2$ is as the optical component in interferometric pressure sensors. The sensitivity of such devices depends critically on two effects: the rate of variation in refractive index (usually a function of volume compressibility) and also the macroscopic path length (a function of linear compressibility). In "ordinary" optical materials, there is an antagonistic relationship between these two factors. A material with a large volume compressibility will tend to have large positive linear compressibilities, so that on increasing pressure the refractive index increases (which acts to increase optical path length), but the material dimensions decrease (which acts to decrease optical path length). Consequently, the overall variation in optical path length with increasing pressure is greatly reduced. The combination of large volume compressibility with a *negative* linear compressibility, however, means that giant NLC materials become more dense at the same time as *increasing* their length in one direction. The two responses now interplay synergically to give order-of-magnitude increases in pressure sensitivity (*3*). Crucially, $Zn[Au(CN)_2]_2$ is also optically transparent over large spectral regions, including at visible wavelengths (*28*). For this specific material, one might also anticipate a strong pressure dependence of its luminescent behaviour, suggesting an alternate mechanism for optical pressure sensing.

On a fundamental level, there are strong implications associated with understanding mechanisms of negative compressibility. A number of biological species are thought to make use of NLC motifs to translate variations in internally-generated hydrostatic pressure into appendage contraction (essentially a fluidic analogue of muscular response): examples include the arms and tentacles of squid, octopus limb movement, and even elephant trunk contraction (*30*). Spiral structures play a crucial role in these systems: crossed helical arrays of tendons or muscle respond to increasing internal pressure (negative external pressure) by contracting along the winding axis. Further mechanical amplification gained from linking small changes in cross-sectional diameter to large variations in length means that these are widely-considered to be very efficient biological structures. By analogy, microporous analogues of $Zn[Au(CN)_2]_2$—making use of *e.g.* metal–organic framework (MOF) chemistry (*31*)—may offer one approach to translating the anomalous mechanical properties of these biological systems into intrinsic material properties: frameworks that contract linearly on guest sorption (*i.e.* "negative sponges") could find use as nanofluidic actuators or as compensators for undesirable moisture-induced swelling of concrete- and clay-based engineering materials.

So how might we design the most extreme NLC candidates? Fortunately, both empirical (*15*) and theoretical (*5*) viewpoints converge on the same set of key design principles. First, one requires anisotropy because NLC requires PLC. Second, the framework should be assembled from rigid struts using nodes with flexible geometries. This guarantees elastic compliances with the requisite large and negative values. And, third, at least one direction of the crystal should be as compressible as possible: maximising PLC maximises NLC. Importantly, what our study of $Zn[Au(CN)_2]_2$ has demonstrated is that the magnitude of NLC achievable is not limited by the energy scale of individual chemical interactions, but only by our collective imagination in developing supramolecular motifs—like the aurophilic helices of $Zn[Au(CN)_2]_2$ —that allow otherwise-inaccessible mechanical responses.

Methods

Synthesis Large single crystals of $Zn[Au(CN)_2]_2$ were prepared hydrothermally. Stoichiometric quantities of $Zn(CH_3COO)_2{\cdot}2H_2O$ (Sigma Aldrich, 98%, 14 mg) and $KAu(CN)_2$ (Sigma Aldrich, 98%, 60 mg) were dissolved in H_2O in a teflon-lined reaction vessel (Parr) (23 mL capacity; 10 mL total solution volume). The vessel was sealed and heated to 120 °C for 2 h, and then cooled slowly to room temperature at a rate of $1\,^{\circ}C\,h^{-1}$. The resulting reaction mixture contained large single crystals of $Zn[Au(CN)_2]_2$ (19.9 mg; 54.1%), which formed as colourless bicapped hexagonal prisms as described in (*23*). Powder samples were prepared by mechanical grinding of single crystals.

Structural characterisation Variable-pressure single-crystal X-ray diffraction measurements were performed using an Agilent Gemini Diffractometer equipped with a Sapphire CCD detector. A single crystal was loaded in a tungsten gasket between the anvils of a Merrill-Bassett diamond anvil cell. A single chip of ruby was included for pressure calibration, and a fluorinated oil was used as pressure transmitting medium. Data were collected at six pressure values between 0 and 1.78 GPa.

Variable-temperature single crystal X-ray diffraction measurements were carried out using an Oxford Diffraction (Agilent) SuperNovae diffractometer (Mo$K\alpha$ radiation) fitted with an nitrogen cryostream. Data were collected at intervals of 50 K on cooling from 300 to 100 K, at intervals of 20 K on heating from 100 to 400 K, and finally at intervals of 50 K on cooling from 400 to 300 K.

Variable-pressure powder diffraction measurements were carried out using the BM01A (Swiss-Norwegian beam line) at the ESRF ($\lambda = 0.69412$ A). A small quantity of finely-ground powder was placed in the cavity of stainless steel gasket of an ETH diamond anvil cell together with a single ruby sphere for pressure calibration and a fluorinated oil as pressure transmitting medium. Data were collected at room temperature and at 18 pressure values between 0 and 14.2 GPa.

Raman spectroscopy Variable-pressure Raman spectroscopy measurements were performed using a membrane diamond anvil cell and a Jobin-Yvon T64000 spectrometer. The 676.4 nm line of a Kr^+ laser was used for excitation. The sample was loaded in the cavity of a stainless steel gasket, together with a single ruby chip as pressure calibrant and glycerol as pressure-transmitting medium.

Acknowledgements

A.B.C. and A.L.G. acknowledge financial support from the E.P.S.R.C. (EP/G004528/2) and the E.R.C. (Grant Ref: 279705), and are grateful to R. I. Cooper and P. J. Saines (Oxford) for assistance. J.H. thanks H. Shepherd, G. Molnar (LCC, Toulouse), D. Maurin (L2C), D. Bourgogne (ICGM), S. Klotz (IMPMC, Paris), K. Murato (Osaka) and D. Granier (ICGM) for technical assistance, and the A.N.R. for financial support (Contract ANR-09-BLAN-0018-01).

Author contributions

A.B.C., J.H. and A.L.G. conceived the study; A.B.C. made the sample; A.B.C., J.C., C.L., J.R., A.v.d.L., A.L.T, V.D., J.H. and A.L.G. performed the experiments; A.B.C., L.P., J.H. and A.L.G. analysed and interpreted the data; A.B.C. and A.L.G. wrote the paper.

Additional information

Correspondence and requests for materials should be addressed to A.L.G.

Competing Financial Interests

The authors declare no competing financial interests.

References

1. Aliev, A. E. *et al.* Giant-stroke, superelastic carbon nanotube aerogel muscles. *Science* **323,** 1575–1578 (2009).
2. Spinks, G. M. *et al.* Pneumatic carbon nanotube actuators. *Adv. Mater.* **14,** 1728–1731 (2002).
3. Baughman, R., Stafstrom, S., Cui, C. & Dantas, S. Materials with negative compressibilities in one or more dimensions. *Science* **279,** 1522–1524 (1998).
4. Newnham, R. E. *Properties of Materials* (Oxford Univ. Press, Oxford, 2005).
5. Grima, J., Attard, D., Caruana-Gauci, R. & Gatt, R. Negative linear compressibility of hexagonal honeycombs and related systems. *Scripta Mater.* **65,** 565–568 (2011).
6. Schmidbauer, H. The aurophilicity phenomenon: a decade of experimental findings, theoretical concepts and emerging applications. *Gold Bull.* **33,** 3–10 (2000).
7. Zhang, H. L. *et al.* Static equation of state of bcc iron. *Phys. Rev. B* **82,** 132409 (2010).
8. McCann, D. R., Cartz, L., Schmunk, R. E. & Harker, Y. D. Compressibility of hexagonal selenium by x-ray and neutron diffraction. *J. Appl. Phys.* **43,** 1432–1436 (1972).
9. Lakes, R. S. Foam structures with a negative Poisson's ratio. *Science* **235,** 1038–1040 (1987).
10. Evans, K. E., Nkansah, M. A., Hutchinson, I. J. & Rogers, S. C. Molecular network design. *Nature* **353**, 124 (1991).
11. Greaves, G. N., Greer, A. L., Lakes, R. S. & Rouxel, T. Poisson's ratio and modern materials. *Nature Mater.* **10,** 823–837 (2011).
12. O'Reilly, J. C., Ritter, D. A. & Carrier, D. R. Hydrostatic locomotion in a limbless tetrapod. *Nature* **386,** 269–272 (1997).
13. Fortes, A. D., Suard, E. & Knight, K. S. Negative linear compressibility and massive anisotropic thermal expansion in methanol monohydrate. *Science* **331,** 742–746 (2011).
14. Li, W. *et al.* Negative linear compressibility of a metal-organic framework. *J. Am. Chem. Soc.* **134,** 11940–11943 (2012).
15. Ogborn, J. M., Collings, I. E., Moggach, S. A., Thompson, A. L. & Goodwin, A. L. Supramolecular mechanics in a metal-organic framework. *Chem. Sci.* **3,** 3011–3017 (2012).
16. Shepherd, H. J. *et al.* Antagonism between extreme negative linear compression and spin crossover in $[Fe(dpp)_2(NCS)_2]\cdot$py. *Angew. Chem. Int. Ed.* **51,** 3910–3914 (2012).
17. Cairns, A. B., Thompson, A. L., Tucker, M. G., Haines, J. & Goodwin, A. L. Rational design of materials with extreme negative compressibility: selective soft-mode frustration in $KMn[Ag(CN)_2]_3$. *J. Am. Chem. Soc.* **134,** 4454–4456 (2012).
18. Lakes, R. & Wojciechowski, K. W. Negative compressibility, negative Poisson's ratio, and stability. *Phys. Status Solidi B* **245,** 545–551 (2008).
19. Gatt, R. & Grima, J. N. Negative compressibility. *Phys. Status Solidi Rapid Res. Lett.* **2,** 236–238 (2008).
20. Nicolaou, Z. G. & Motter, A. E. Mechanical metamaterials with negative compressibility transitions. *Nature Mater.* **11,** 608–613 (2012).
21. Sears, D. R. & Klug, H. P. Density and expansivity of solid xenon. *J. Chem. Phys.* **37,** 3002–3006 (1962).
22. Hoskins, B. F., Robson, R. & Scarlett, N. V. Y. Six interpenetrating quartz-like nets in the structure of $ZnAu_2(CN)_4$. *Angew. Chem. Int. Ed.* **34,** 1203–1204 (1995).
23. Katz, M. J., Ramnial, T., Yu, H.-Z. & Leznoff, D. B. Polymorphism of $Zn[Au(CN)_2]_2$ and Its luminescent sensory response to NH_3 vapor. *J. Am. Chem. Soc.* **130,** 10662–10673 (2008).
24. Goodwin, A. L., Kennedy, B. J. & Kepert, C. J. Thermal expansion matching via framework flexibility in zinc dicyanometallates. *J. Am. Chem. Soc.* **131,** 6334–6335 (2009).
25. O'Grady, E. & Kaltsoyannis, N. Does metallophilicity increase or decrease down group 11? Computational investigations of $[Cl–M–PH_3]_2$ (M = Cu, Ag, Au, [111]). *Phs. Chem. Chem. Phys.* **6,** 680–687 (2004).
26. Cliffe, M. J. & Goodwin, A. L. PASCal: A principal-axis strain calculator for thermal expansion and compressibility determination. *J. Appl. Cryst.* **45,** 1321–1329 (2012).
27. Chapman, K. W. & Chupas, P. J. Pressure enhancement of negative thermal expansion behavior and induced framework softening in zinc cyanide. *J. Am. Chem. Soc.* **129,** 10090–10091 (2007).
28. Korǿok, J. L., Katz, M. J. & Leznoff, D. B. Impact of metallophilicity on "colossal" positive and negative thermal expansion in a series of isostructural dicyanometallate coordination polymers. *J. Am. Chem. Soc.* **131,** 4866–4871 (2009).
29. Goodwin, A. L., Keen, D. A. & Tucker, M. G. Large negative linear compressibility of $Ag_3[Co(CN)_6]$. *Proc. Natl. Acad. Sci. U.S.A.* **105,** 18708–18713 (2008).
30. Kier, W. M. & Smith, K. K. Tongues, tentacles and trunks: the biomechanics of movement in muscular-hydrostats. *Zool. J. Linn. Soc.* **83,** 307–324 (1985).
31. Sun, J. *et al.* QMOF-1 and QMOF-2: three-dimensional metalÐorganic open frameworks with a quartzlike topology. *Angew. Chem. Int. Ed.* **41,** 4471–4473 (2002).